ISSN 1068-3755, Surface Engineering and Applied Electrochemistry, 2025, Vol. 61, No. 5, pp. 793–803. © Allerton Press, Inc., 2025.
Russian Text © The Author(s), 2025, published in Elektronnaya Obrabotka Materialov, 2025, No. 3, pp. 12–23.

Structure, Mechanical, and Corrosion Properties of Coatings Based on ZrN Solid Solution

N. N. Cherenda[a], S. N. Grigoriev[b], A. V. Basalai[c, *], N. V. Bibik[a], A. A. Vereschaka[d], A. Yu. Izobello[c], O. V. Reva[e], D. P. Rusalsky[a], A. K. Kuleshov[a], V. V. Uglov[a], and S. I. Bahayeu[c]

[a] *Belarusian State University, Minsk, 220030 Republic of Belarus*
[b] *Moscow State Technological University STANKIN, Moscow, 127055 Russia*
[c] *Physical-Technical Institute, National Academy of Sciences of Belarus, Minsk, 220084 Republic of Belarus*
[d] *Institute of Design and Technological Informatics, Russian Academy of Sciences, Moscow, 127055 Russia*
[e] *University of Civil Defense, Ministry of Emergency Situations of the Republic of Belarus, Minsk, 220118 Republic of Belarus*
**e-mail: anna.basalay@mail.ru*

Received May 12, 2025; revised May 27, 2025; accepted May 29, 2025

Abstract—The structure, elemental composition, and mechanical and corrosion properties of (Zr, Nb)N, (Zr, Hf)N and (Zr, Nb, Hf)N vacuum-arc coatings deposited on the titanium alloy Ti–6Al–4V were studied. The X-ray diffraction analysis, scanning electron microscopy, microhardness measurement, adhesion, and corrosion tests were used as investigation techniques. It was found that the coatings were single-phase solid solutions based on ZrN. The highest microhardness value (17 GPa) was observed for the (Zr, Hf, Nb)N coating, and the lowest value (9 GPa) for the (Zr, Nb)N coating. The (Zr, Hf)N coating also possessed the highest critical force Lc3 during scratch tests. Comparison with the data obtained earlier showed that a decrease of the Nb concentration in the (Zr, Nb)N coating and an increase of the Hf concentration in the (Zr, Hf)N coating led to the growth of the critical force Lc3. Corrosion tests carried out in a 3% NaCl solution in the galvanostatic mode showed that the (Zr, Nb)N coating maintained continuity over the entire surface of the alloy in contrast to the coatings containing Hf atoms.

Keywords: titanium alloy, biomedical implants, nitride coatings, adhesion, microhardness, corrosion
DOI: 10.3103/S1068375525700875

INTRODUCTION

Titanium alloys are widely used for the production of metal implants [1–5]. At the same time, they are foreign bodies introduced into the human body and can cause a corresponding reaction of the immune and other systems [4]. For example, the Ti–6Al–4V alloy, widely used to make implants, contains potentially toxic atoms of aluminum and vanadium that pose a risk of entering the human body [3, 4, 6]. Vanadium ingestion can lead to problems with the gastrointestinal tract, for example [4]. Aluminum is also toxic in high doses and has been linked to a number of health conditions, including neurotoxicity, impaired motor function, decreased spatial memory, and Alzheimer's disease [4].

The application of protective coatings is one of the most widely used approaches to eliminate the negative effects of using this alloy [7–9]. In this area, the application of PVD coatings of transition metal nitrides has attracted considerable attention [9, 10]. Such coatings have exceptional mechanical and tribological properties as well as high corrosion resistance [9, 10]. ZrN coating is one example of this kind [7, 8, 11, 12]. In particular, ZrN coatings are commercially available coatings for orthopaedic implants, which are used for articulating surfaces in joint replacement surgeries [7]. In addition to binary nitride materials, ternary and more complex coatings are being developed to provide an optimal combination of properties [13, 14]. With this approach, coatings of Zr–Nb–N and Zr–Hf–N compositions are of undoubted interest [13–24].

A number of studies have reported that PVD coatings and Zr–Nb–N films have high hardness, elastic modulus and wear resistance [15–17]. It was mentioned in [15, 16] that the Zr–Nb–N system has great potential for forming coatings with high adhesive strength. In most of the cases considered, the ZrN-based FCC solid solution is mentioned as the sole or main phase constituent of the coating [16, 17]. At the same time, changing the concentration of Nb leads to structural changes in the coating, affecting its mechanical properties [17, 18]. It was found in [17] that the addition of niobium causes a refinement of the coating structure. This effect was also found for Nb–Zr–N films [18]. An increase in the stoichiometric ratio of Zr to Nb leads to an increase in the average grain size and lattice parameter [18]. Zr–Hf–N coatings also have an FCC crystal lattice and are character-

ized by improved mechanical and tribological properties [20–23]. At the same time, it was reported that increasing the concentration of Hf in the coating does not lead to a significant change in hardness [20–22]. The slight strengthening of the solid solution due to the small difference in the atomic radii of Zr and Hf may be the main reason for this effect [20]. The small difference in atomic radii is also the reason for the minor influence of Hf atoms (up to 11.9 at % Hf) on the level of residual stresses of ZrN films [24]. On the contrary, an increase in the concentration of Hf significantly increases the adhesive strength of coatings and their wear resistance [20, 21]. The positive effect of Hf additive on the corrosion resistance, tribological performance and biocompatibility of ZrCN coating was reported in [25].

Previously conducted studies of the mechanical and corrosion properties of ZrN, (Zr, Ti)N, (Zr, Hf)N, (Zr, Nb)N, (Ti, Zr, Hf)N, and (Ti, Zr, Nb)N coatings applied to the titanium alloy Ti–6Al–4V showed that the presence of Hf atoms in the coating leads to an increase in the hardness and adhesion of the coating [26], while the presence of Nb atoms provides higher corrosion resistance during electrochemical corrosion [26]. The main objective of this work was to study the influence of Nb and Hf atoms on the structure and mechanical and corrosion properties of (Zr, Hf)N, (Zr, Nb)N, (Zr, Nb, Hf)N coatings.

EXPERIMENTAL PROCEDURE

Samples of titanium alloy Ti–6Al–4V (Grade 5) were used for the research. The coatings were applied by vacuum arc deposition with controlled movement of the cathode spot in a nitrogen atmosphere using a modernized VIT-2 installation [27, 28]. The method of controlled movement of the cathode spot is characterized by a decrease in the amount of microparticles of the droplet phase compared to traditional arc-type evaporators. Before deposition, the surface was cleaned with Zr ions, resulting in the formation of a thin (~50 nm) metallic sublayer on the substrate. The coatings were applied using two metal cathodes. The following cathode pairs were used: Zr and 50 at % Zr–50 at % Nb, Zr and 50 at % Zr–50 at % Hf, 50 at % Zr–50 at % Nb and 50 at % Zr–50 at % Hf. The cathodes used were made from cast alloys of appropriate compositions. As a result, the following coatings were deposited: (Zr, Nb)N, (Zr, Hf)N, and (Zr, Nb, Hf)N. The use of a second Zr cathode allows for reducing the concentration of Nb and Hf in the (Zr, Nb)N and (Zr, Hf)N coatings, in contrast to the coatings studied in [29]. During coating deposition, the arc current of the zirconium cathode was 80 A. The arc current of the Zr–Nb and Zr–Hf cathodes was 85 and 90 A, respectively. The deposition was carried out under the following parameters, the same for all processes: nitrogen pressure of 0.42 Pa, substrate bias voltage of –150 V, sample holder rotation speed of 0.7 rpm.

The structural and phase state of the coatings was studied using a Rigaku Ultima IV diffractometer in Cu Kα radiation. Analysis of the elemental composition and cross-sectional morphology of the coatings was carried out using a LEO1455VP scanning electron microscope. Analysis of the elemental composition and surface morphology of coating sections after corrosion tests was carried out using a TESCAN MIRA 3 LMH electron microscope. The microhardness of the coatings was determined on a 402MVD microhardness tester using a Vickers indenter. The normal load on the diamond indenter was 1 N, the holding time in the loaded state was 10 s. Adhesion tests were carried out by scratching using a diamond indenter with a radius of 0.4 mm, the load on which increased linearly from 0.05 to 98 N. The track length was 15 mm (loading rate 0.17 kg/s, sample movement speed 0.19 mm/s). Three tests were performed on each sample.

Tests for corrosion resistance of nitride coatings were carried out on an Autolab/PGSTAT302N potentiostat/galvanostat in galvanostatic mode.

In this mode, a constant current load of 4 mA was applied to the coating (anode). A saturated silver chloride electrode served as the reference electrode, and a platinum plate served as the counter electrode. The working surface area of each coating was 1 cm^2. All tests were carried out in a 3% NaCl solution at room temperature and without convection. The test time was 400 s.

RESULTS AND DISCUSSION

The results of the analysis of the elemental composition of the coatings in the surface layer with a thickness of ~1 μm are presented in Table 1. It can be seen that the predominant metallic element in multicomponent coatings is zirconium. The use of two cathodes (one of which is Zr) in (Zr, Nb)N and (Zr, Hf)N coatings makes it possible to reduce the concentration of niobium and hafnium in the solid solution based on ZrN to 10.2 and 2.0 at %, respectively. Previously obtained data showed that the use of one Zr–Nb or Zr–Hf cathode leads to the formation of (Zr, Nb)N and (Zr, Hf)N coatings with a concentration of 23.5 at % Nb and 5.7 at % Hf [29]. Thus, a comparative analysis of the data obtained in this work with the data of the work [29] allows us to trace the influence of niobium and hafnium concentration on the properties of coatings. The concentration of Nb and Hf in the (Zr, Nb, Hf)N coating was higher than in the case of (Zr, Nb)N and (Zr, Hf)N coatings. However, this difference is insignificant and is within the limits of error in

Table 1. Concentration of elements in (Zr,Nb)N, (Zr,Hf)N and (Zr,Nb,Hf)N coatings (energy dispersive microanalysis)

Coating	Concentration of elements, at %			
	Zr	Nb	Hf	N
(Zr, Nb)N	41.1	10.2	–	48.7
(Zr, Hf)N	49.4	–	2.0	48.6
(Zr, Nb, Hf)N	38.5	11.5	3.3	46.7

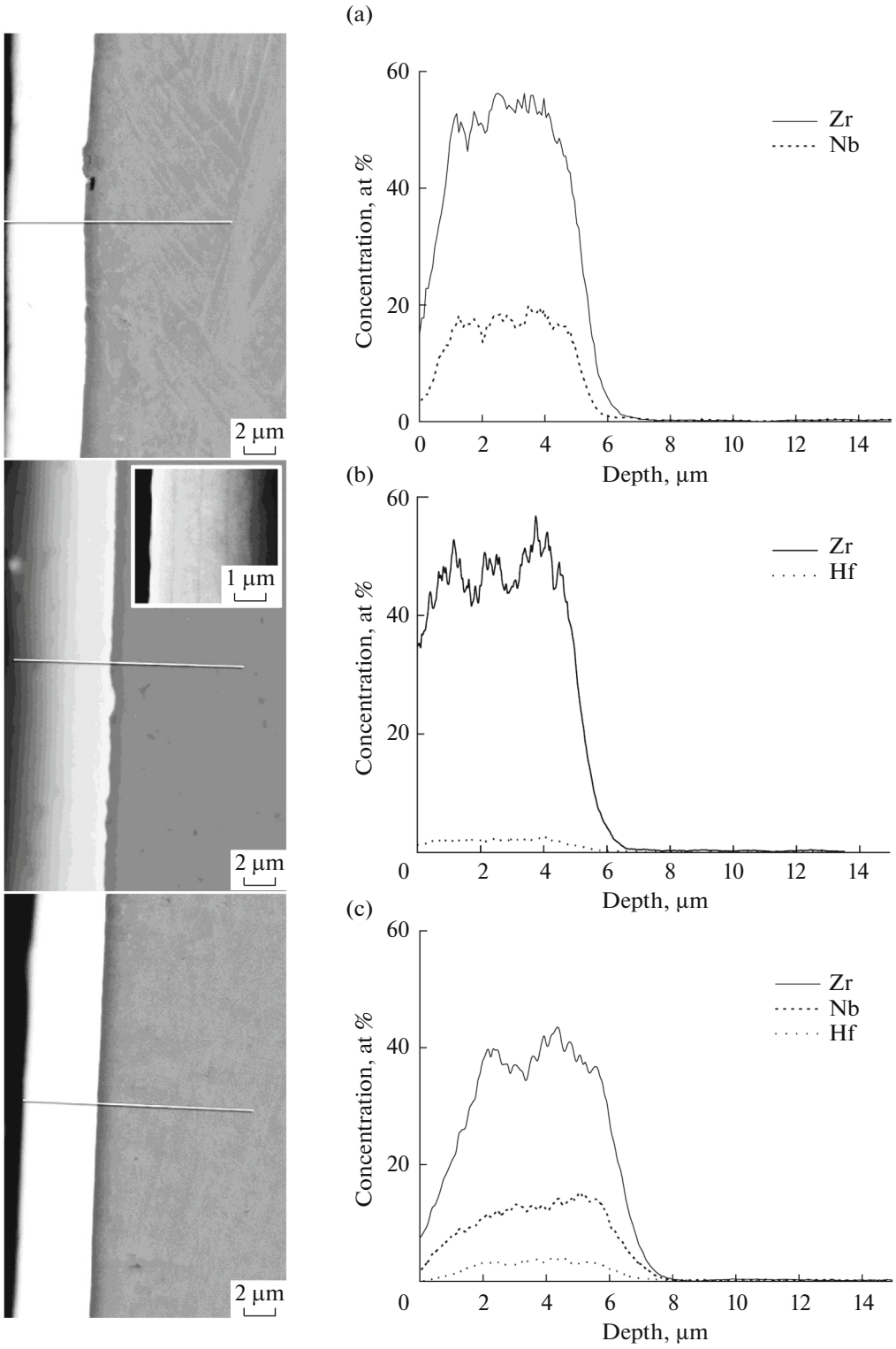

Fig. 1. Cross-sectional morphology and element distribution by depth of samples coated with (a) (Zr, Nb)N, (b) (Zr, Hf)N, and (c) (Zr, Nb, Hf)N.

determining the concentration. For all types of coatings, the nitrogen concentration was close to stoichiometric (47–49 at %).

The morphology of the cross-sections of the coatings and the distribution of elements by depth are represented in Fig. 1. As can be seen, the coating thick-

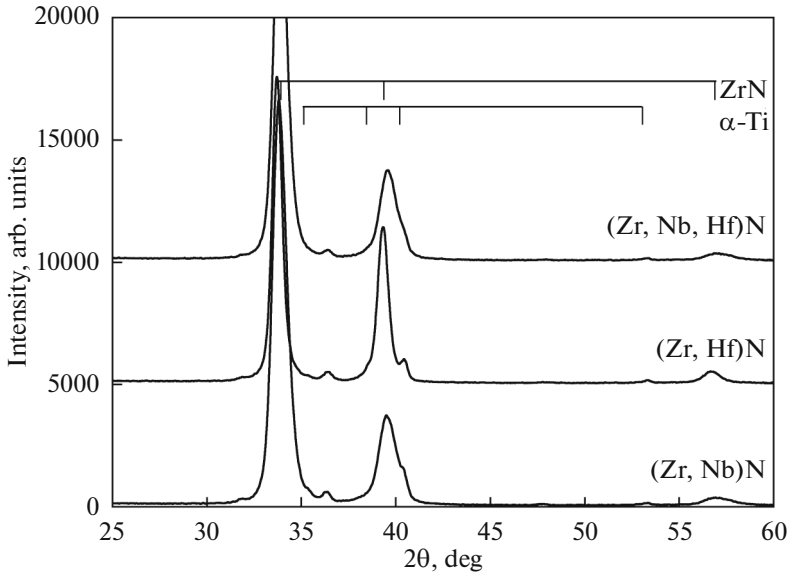

Fig. 2. Sections of diffraction patterns of samples with (Zr, Nb)N, (Zr, Hf)N, and (Zr, Nb, Hf)N coatings.

ness is ~4.5 μm. In the (Zr, Hf)N coating (insert in Fig. 1b), the multilayer structure that arose due to the rotation of the samples during the deposition process is clearly visible. It is obvious that such a multilayer structure should be characteristic of all types of coatings under consideration. However, the sensitivity of the used equipment did not allow the structure to be identified in all cases. At the same time, some differences are observed between the average concentration by thickness (Fig. 1) and the concentration of elements in the surface layer (as can be seen in Table 1). The average concentration of Nb across the thickness of the (Zr, Nb)N coating was 16.2 at %. In the (Zr, Nb, Hf)N coating, the Nb concentration was 12–14 at %. The concentration of Hf in the coatings changed slightly.

The diffraction patterns of samples with (Zr, Hf)N, (Zr, Nb)N and (Zr, Nb, Hf)N coatings are represented in Fig. 2. As can be seen from Fig. 2, in these experiments, the patterns obtained earlier are observed [29]. In particular, during deposition, single-phase coatings based on a ZrN solid solution with an FCC crystal lattice containing additional alloying elements were formed. The diffraction lines of the ZrN-based solid solution had a larger width in the (Zr, Nb)N and (Zr, Nb, Hf)N coatings compared to the (Zr, Hf)N coating. This effect can be associated with both the greater magnitude of microstresses in the coatings and the smaller size of the crystallites. The latter effect was observed in [17, 18]. The diffraction patterns of all coatings show the presence of a diffraction line ($2\theta = 36.2°$), corresponding to α-Zr, which is associated with the formation of an intermediate metallic sublayer during ion cleaning.

In addition, depending on the type of coatings, a shift in the diffraction lines of solid solutions based on ZrN is observed, which is associated with a change in the lattice parameter of the solid solutions. In particular, the use of the Zr–Nb cathode led to a shift of the diffraction lines to the region of smaller angles, that is, to a decrease in the lattice parameter of the solid solution to 0.4586 ± 0.006 nm in the (Zr, Nb)N coating compared to the (Zr, Hf)N coating (0.4604 ± 0.006 nm). The reason for this effect is that the atomic radius of Nb (0.164 nm) is smaller than the atomic radius of Zr (0.175 nm). A similar pattern was observed in [17]. The lattice parameter of the solid solutions corresponds (within the error limits) to the lattice parameter in the ZrN coating (0.4591 ± 0.005 nm) [29]. Comparison with work data [29] shows that a decrease in the hafnium concentration in the coating from 5.7 to 2 at % led to a slight decrease in the lattice parameter to a value corresponding to the lattice parameter in the ZrN coating. At the same time, the concentration of niobium decreased from 23.5 to 16.2 at % (according to the data obtained from the analysis of cross sections), leading to a significant increase in the lattice parameter up to the value of the lattice parameter of ZrN. In general, a decrease in the concentration of niobium and hafnium should lead to a decrease in micro- and macrostresses in the coatings and a corresponding change in mechanical characteristics. The lattice parameter of the solid solution in the coating (Zr, Nb, Hf)N (0.4582 ± 0.006 nm) within the error limits does not differ from the lattice parameter of the solid solution in the coating (Zr, Nb)N, which is associated with an insignificant change in the elemental composition of the coatings (see Table 1).

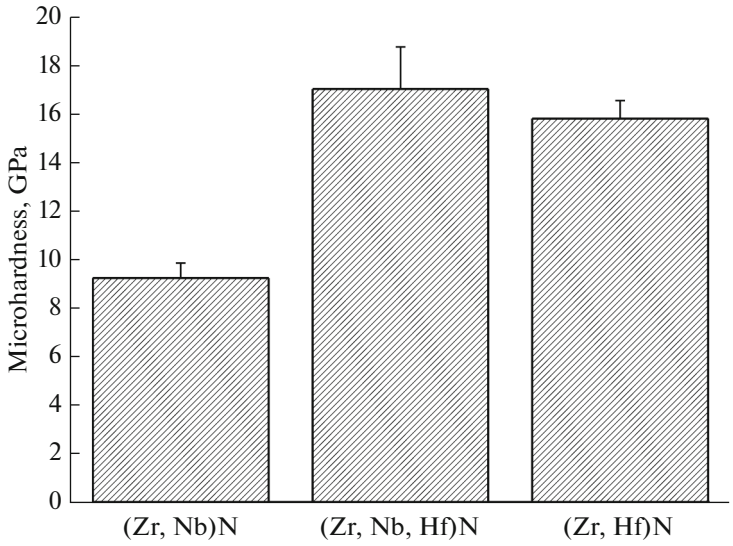

Fig. 3. Microhardness of (Zr, Nb)N, (Zr, Hf)N, and (Zr, Nb, Hf)N coatings.

The mechanical properties of (Zr, Nb)N, (Zr, Hf)N and (Zr, Nb, Hf)N coatings were also investigated. The results of Vickers microhardness measurements are represented in Fig. 3. The penetration depth of the indenter was 1.5–2 μm. As can be seen from Fig. 3, the highest microhardness value (16–17 GPa) is observed in (Zr, Hf)N and (Zr, Nb, Hf)N coatings, which have a similar elemental composition (see Table 1). The microhardness of the (Zr,Nb)N coating is 9 GPa. The obtained data are consistent with previously conducted studies, which found that (Zr, Nb)N coatings have lower microhardness compared to other types of coatings, which may be due to the presence of tensile stresses in it [26].

Data on measuring the Knoop microhardness of ZrN, (Zr, Nb)N coatings with an Nb concentration of 23.5 at % and (Zr, Hf)N coatings with an Hf concentration of 5.7 at % were presented in [26]. The microhardness values were 21.5, 12.0, and 28.3 GPa, respectively [26]. Direct comparison with the data obtained in the present work is incorrect since different types of indenters and different loads were used. However, it is possible to estimate the influence of the composition on the microhardness value through the ratio of the maximum microhardness observed in the (Zr, Hf)N coating to the minimum microhardness obtained for the (Zr, Nb)N coating. For the case presented in [26], this ratio was 2.4. At the same time, for the coatings studied in this work, this ratio decreased to 1.9. Thus, a decrease in the concentration of Nb and Hf in the (Zr, Nb)N and (Zr, Hf)N coatings should obviously lead to a decrease in the considered microhardness ratio to a value of 1, and the microhardness value itself will approach the value of the ZrN coating.

For the studied types of coatings, tests were also conducted for their adhesive strength. All scratches were applied along the grinding direction of the samples. The results showed that scratches are characterized by the appearance of chips along the edges followed by complete peeling (abrasion) of the coating. It is known that three main critical loads can be determined using the method: Lc1, corresponding to the appearance of initial cracks in the scratch; Lc2, corresponding to the first chip along the edges of the scratch; and Lc3, corresponding to complete peeling (abrasion) of the coating [30]. In these experiments, the critical force Lc3 was determined using optical microscopy based on the distance at which complete delamination occurred and on the dependence of the applied load on the friction path of the diamond indenter. The conducted studies showed that the critical force Lc3 was 36 N for samples with a (Zr, Nb)N coating, 50 N for a (Zr, Hf)N coating, and 42 N for a (Zr, Nb, Hf)N coating. Another criterion for complete peeling of a coating applied to relatively smooth surfaces can be a sharp change in the value of the friction coefficient of the diamond indenter during scratch tests [31]. The dependences of the indenter friction coefficient on the friction path are shown in Fig. 4. A sharp increase in the friction coefficient at a certain section of the path indicates complete peeling (abrasion) of the coating and penetration of the indenter into the Ti–6Al–4V alloy. The data obtained in this way correspond to the values of the critical force Lc3 determined using optical microscopy.

The highest values of the critical force Lc3 were observed for samples with coatings containing hafnium. However, as can be seen from the photographs of areas where the coating has peeled off (worn off) (Fig. 5), these coatings are characterized by the largest chips at the edges of the scratch.

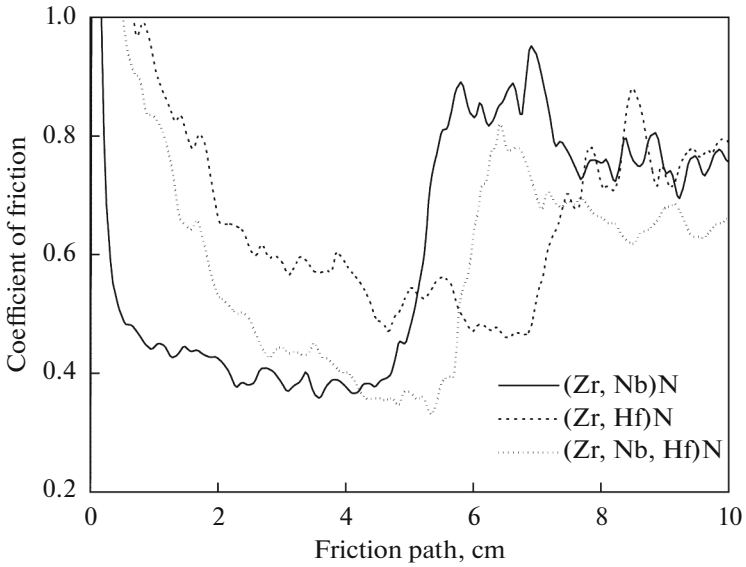

Fig. 4. Dependence of the friction coefficient of a diamond indenter on the friction path for samples with (Zr, Nb)N, (Zr, Hf)N, and (Zr, Nb, Hf)N coatings.

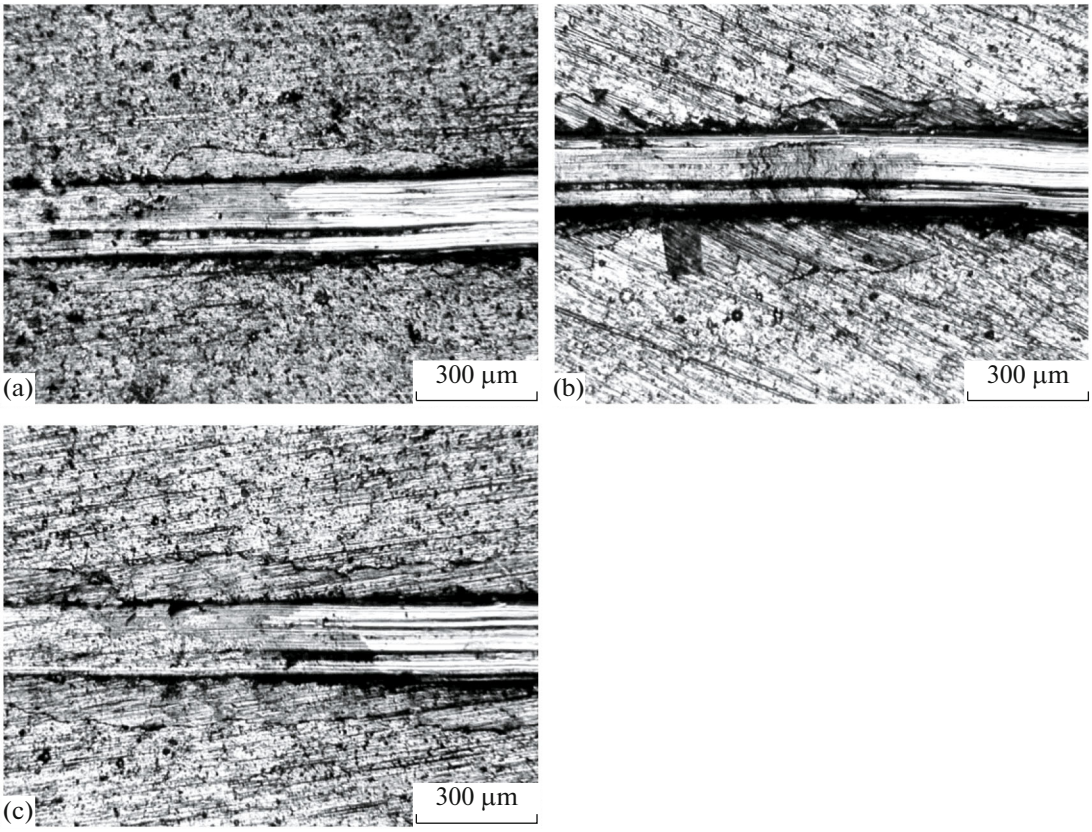

Fig. 5. Surface morphology (optical microscopy) of samples with coatings in areas of complete coating peeling: (a) (Zr, Nb)N, (b) (Zr, Hf)N, and (c) (Zr, Nb, Hf)N.

Adhesion tests of ZrN, (Zr, Nb)N coatings with a Nb concentration of 23.5 at % and (Zr, Hf)N coatings with a Hf concentration of 5.7 at % were carried out in [26] under the same conditions as in the present case. The critical force values for these coatings were 37.3, 33.4, and 54.0 N, respectively [26]. Comparison with

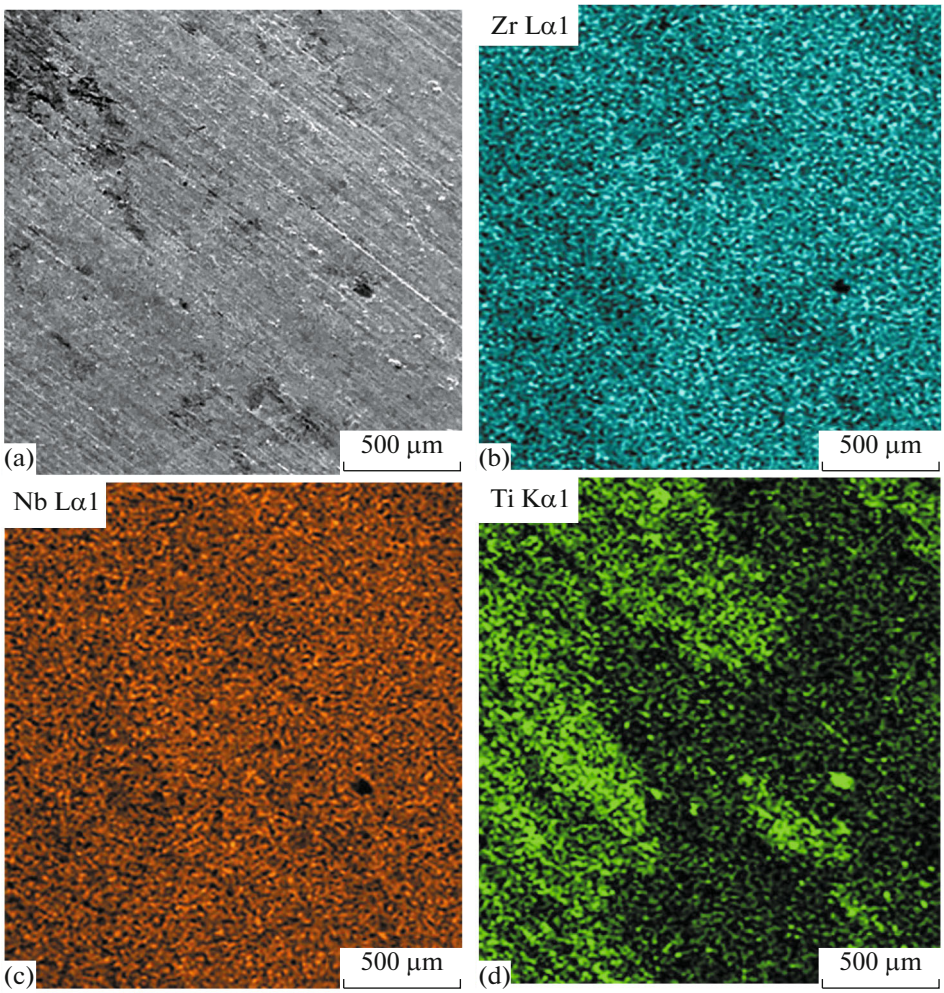

Fig. 6. Morphology of the corroded area of the (a) (Zr, Nb)N coating and (b–d) the corresponding maps of the distribution of elements by area.

the data obtained in our work shows that a decrease in the niobium concentration in the (Zr, Nb)N coating and an increase in the hafnium concentration in the (Zr, Hf)N coating led to an increase in the critical force Lc3. These data correlate with previous studies [26], which showed that the presence of Nb in the ZrN coating leads to a decrease in the adhesive strength. A possible reason for this effect is the occurrence of tensile residual stresses in the crystal lattice of the coating [29], which contribute to the destruction of the coating under mechanical loads. While the presence of Hf, on the contrary, leads to an increase in the adhesive strength and hardness of the coating. The positive effect of Hf atoms on the adhesion strength of ZrN coatings was found in [20, 21]. However, the large difference in the strength characteristics of the titanium alloy as a substrate and the hard coating in this case leads to the coating being pressed through by the indenter and an increase in the area of coating chips along the scratch. The (Zr, Nb, Hf)N coating had a kind of "average" mechanical characteristics due to the "opposite" influence of Nb and Hf atoms on the mechanical properties of coatings based on ZrN solid solutions.

Previous studies of the corrosion properties of coatings in aggressive environments have shown that coatings based on ZrN solid solutions exhibit high corrosion resistance in solutions with acidic (H_2SO_4), alkaline (NaOH), and neutral (NaCl) environment at 50°C [29]. Tests under the action of forced electric potential in a NaCl solution also showed high corrosion resistance of the coatings [29]. However, it was found that the difference in the corrosion characteristics of the coatings was insignificant. Therefore, to determine the influence of the composition of the (Zr, Nb)N, (Zr, Hf)N and (Zr, Nb, Hf)N coatings on the corrosion properties and nature of destruction in a 3% NaCl solution, a galvanostatic mode with a high constant current load was used. Following this, an analysis of the morphology and elemental composition of the areas

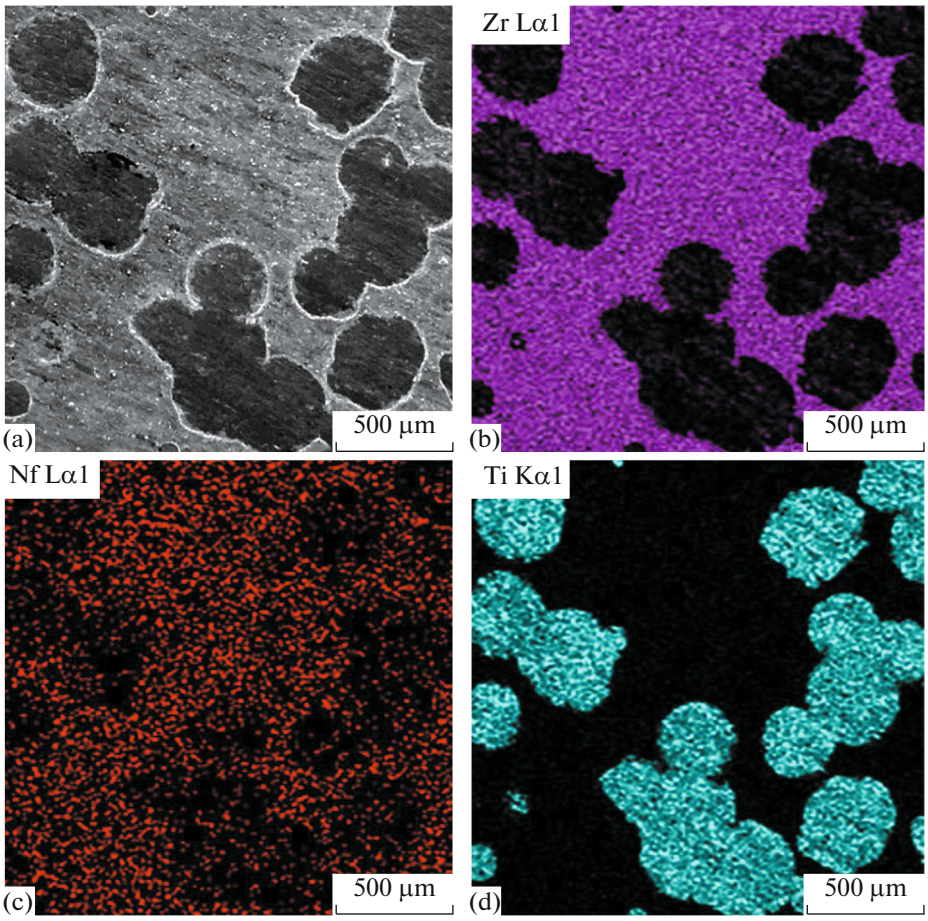

Fig. 7. Morphology of the corroded area of the (a) (Zr, Hf)N coating and (b–d) the corresponding maps of the distribution of elements by area.

subject to corrosion was carried out. The results of the research are represented in Figs. 6–8.

The surface morphology of a section of the (Zr, Nb)N coating subjected to corrosion and a map of the distribution of elements over the surface of this section are represented in Fig. 6. It can be seen that the (Zr, Nb)N coating is preserved over the entire surface of the analyzed area according to the Zr and Nb distribution map. This distribution indicates that the corrosion was continuous. The presence of a titanium signal on the distribution map may be due to a decrease in the coating thickness to a value smaller than the region of generation of characteristic X-ray radiation and excitation of atoms of the surface layer of the substrate. The distribution of characteristic X-ray radiation of Ti atoms is nonuniform, which may be due to the nonuniform nature of continuous corrosion.

It was shown in Fig. 7 that corrosion was characterized by a pitting nature in the (Zr, Hf)N coating. The corrosion lesions in the surface plane were round in shape and penetrated the entire thickness of the coating down to the substrate. The cause of the pitting lesions could be a droplet metal phase [29], the density of which on the surface correlated with the density of corrosion foci obtained in this work. It is known that the mechanism of corrosion destruction of metal nitride coatings is strongly influenced by such defects as macroparticles and pores [32]. The metal droplets act as anodes in relation to the coating material, forming galvanic pairs that accelerate local corrosion [32]. Interaction of a locally exposed metal surface with aggressive anions (Cl^-) can also be the cause of pitting corrosion [26].

The surface morphology of a section of the (Zr, Nb, Hf)N coating subjected to corrosion and a map of the distribution of elements over the surface of this section are represented in Fig. 8. It is evident from Fig. 8 that the corrosion has a mixed character with features inherent in both (Zr, Nb)N coatings and (Zr, Hf)N coatings: dissolution of the coating over relatively large areas and the formation of pits.

It should be noted that the droplet phase was present on the surface of all types of coatings, but pitting corrosion was detected only on samples with a (Zr, Hf)N coating as well as earlier on ZrN coatings [26]. Therefore, the predominant corrosion mechanism

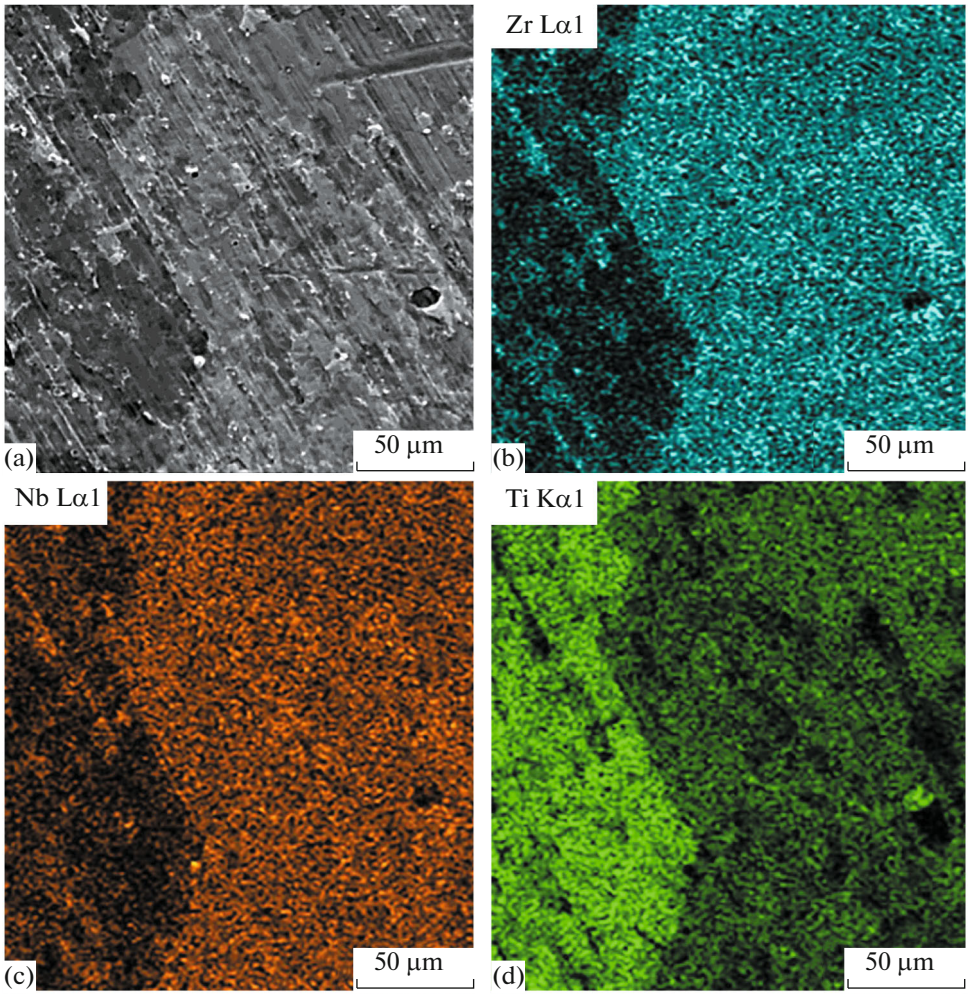

Fig. 8. Morphology of the corroded area of the (a) (Zr,Nb,Hf)N coating and (b–d) the corresponding maps of the distribution of elements by area. The Hf distribution map is not shown due to the low concentration of Hf (similar to that shown in Fig. 8b).

will depend not only on the presence of the metallic droplet phase but also on the structure and electrochemical properties of the coating, in particular on its potential under the given corrosion test conditions.

Corrosion tests showed that the (Zr, Nb)N coating demonstrated the best resistance under test conditions and ensured the preservation of the coating continuity over the entire area, unlike the (Zr, Hf)N and (Zr, Nb, Hf)N coatings. The (Zr, Nb)N and (Zr, Hf)N coatings have different corrosion patterns. By analogy with the mechanical properties, the (Zr, Nb, Hf)N coating demonstrated during testing features characteristic of both (Zr, Nb)N and (Zr, Hf)N coatings.

CONCLUSIONS

In this paper, the structure, elemental composition, and mechanical and corrosion properties of (Zr, Nb)N, (Zr, Hf)N and (Zr, Nb, Hf)N coatings, which were applied using two cathodes on a Ti–6Al–4V titanium alloy substrate by vacuum arc deposition, were investigated. The coatings were single-phase solid solutions based on ZrN with an FCC crystal structure. The coatings containing Nb had a smaller lattice parameter compared to the ZrN standard, which is associated with the smaller atomic radius of the niobium atoms. Comparison with previously conducted studies showed that an increase in the niobium concentration leads to a decrease in the lattice parameter of the ZrN-based solid solution.

The Vickers microhardness of the (Zr, Hf)N and (Zr, Nb, Hf)N coatings was 16–17 GPa. The microhardness of the (Zr, Nb)N coating was lower: ~9 GPa. In the adhesion tests by the scratch method, the highest critical force Lc3 was observed for the (Zr, Hf)N coating. However, the coatings containing Hf were characterized by the largest chipping area along the scratch edges. The (Zr, Nb)N coating showed a relatively small critical load value, which may be due to the presence of tensile stresses in the ZrN solid solution. A

decrease in the niobium concentration in the (Zr, Nb)N coating and an increase in the hafnium concentration in the (Zr, Hf)N coating leads to an increase in the critical force Lc3.

Corrosion tests of coatings were carried out in galvanostatic mode in a 3% NaCl solution. It was established that the (Zr, Nb)N coating maintains continuity over the entire surface of the analyzed area under test conditions. The corrosion of the (Zr, Hf)N coating was of a point nature. The corrosion lesions in the surface plane were round in shape and penetrated the entire thickness of the coating down to the substrate. The corrosion of the (Zr, Nb, Hf)N coating is of a mixed nature with features typical of both (Zr, Nb)N and (Zr, Hf)N coatings: dissolution of the coating over relatively large areas and the formation of pits.

FUNDING

This work was supported by the Belarusian Republican Foundation for Basic Research (project no. T23RNF-228) and the Russian Science Foundation (project no. 23-49-10038).

CONFLICT OF INTEREST

The authors of this work declare that they have no conflicts of interest.

REFERENCES

1. Annur, D., Kartika, I., Supriadi, S., and Suharno, B., Titanium and titanium based alloy prepared by spark plasma sintering method for biomedical implant applications, *Mater. Res. Expr.,* 2021, vol. 8, p. 012001. https://doi.org/10.1088/2053-1591/abd969
2. Brunello, G., Brun, P., Gardin, C., Ferroni, L., et al., Biocompatibility and antibacterial properties of zirconium nitride coating on titanium abutments: An in vitro study, *PLoS ONE,* 2018, vol. 13, p. e0199591. https://doi.org/10.1371/journal.pone.0199591
3. Chen, Q. and Thouas, G.A., Metallic implant biomaterials, *Mater. Sci. Eng. R,* 2015, vol. 87, p. 1. https://doi.org/10.1016/j.mser.2014.10.001
4. Kaur, M. and Singh, K., Review on titanium and titanium based alloys as biomaterials for orthopaedic applications, *Mater. Sci. Eng. C,* 2019, vol. 102, p. 844. https://doi.org/10.1016/j.msec.2019.04.064
5. Sarraf, M., Rezvani Ghomi, E., Alipour, S., Ramakrishna, S., et al., A state-of-the-art review of the fabrication and characteristics of titanium and its alloys for biomedical applications, *Bio-Des. Manuf.,* 2022, vol. 5, p. 371. https://doi.org/10.1007/s42242-021-00170-3
6. Chen, H., Feng, R., Xia, T., Wen, Z., et al., Progress in surface modification of titanium implants by hydrogel coatings, *Gels,* 2023, vol. 9, p. 423. https://doi.org/10.3390/gels9050423
7. Gabor, R., Cvrček, L., Kudrnová, M., Hlinka, J., et al., ZrN coating as a source for the synthesis of a new hybrid ceramic layer, *Appl. Surf. Sci. Adv.,* 2024, vol. 22, p. 100615. https://doi.org/10.1016/j.apsadv.2024.100615
8. Rabadzhiyska, S., Dechev, D., Ivanov, N., Ivanova, T., et al., Wear and corrosion resistance of ZrN coatings deposited on Ti6Al4V alloy for biomedical applications, *Coatings,* 2024, vol. 14, p. 1434. https://doi.org/10.3390/coatings14111434
9. Wu, X., Han, H., Jiang, Y., Zhu, D., et al, Opportunities and challenges of the nitride coatings for artificial implants, *Surf. Coat. Technol.,* 2024, vol. 480, p. 130587. https://doi.org/10.1016/j.surfcoat.2024.130587
10. Al-Asadi, M. and Al-Tameemi, H., A review of tribological properties and deposition methods for selected hard protective coatings, *Tribol. Int.,* 2022, vol. 176, p. 107919. https://doi.org/10.1016/j.triboint.2022.107919
11. Laera, A.M., Massaro, M., Dimaio, D., Vencl, A., et al., Residual stress and tribological performance of ZrN coatings produced by reactive bipolar pulsed magnetron sputtering, *Materials,* 2021, vol. 14, p. 6462. https://doi.org/10.3390/ma14216462
12. Savostikov, V.M., Leonov, A.A., Denisov, V.V., Denisova, Yu.A., et al., Formation of a Zr+Zr_xN_y+(Zr+TiBSiNi)N+(TiBSiNi)N gradient-layered coating based on physical and tribotechnical characteristics of constituent layers, *Russ. Phys. J.,* 2024, vol. 67, p. 1090. https://doi.org/10.1007/s11182-024-03220-2
13. Klostermann, H., Fietzke, F., Labitzke, R., Modes, T., et al., Zr–Nb–N hard coatings deposited by high power pulsed sputtering using different pulse modes, *Surf. Coat. Technol.,* 2009, vol. 204, p. 1076. https://doi.org/10.1016/j.surfcoat.2009.09.012
14. Kanoun, M. and Goumri-Said, S., Effect of alloying on elastic properties of ZrN based transition metal nitride alloys, *Surf. Coat. Technol.,* 2014, vol. 255, p. 140. https://doi.org/10.1016/j.surfcoat.2014.03.048
15. Zhang, S., Wang, N., Li, D.J., Dong, L., et al., The synthesis of Zr–Nb–N nanocomposite coating prepared by multi-target magnetron co-sputtering, *Nucl. Instrum. Methods Phys. Res., Sect. B,* 2013, vol. 307, p. 119. https://doi.org/10.1016/j.nimb.2012.12.067
16. Wu, Z.T., Qi, Z.B., Jiang, W.F., Wang, Z.C., et al., Influence of niobium addition on microstructure, mechanical properties and oxidation resistance of ZrN coatings, *Thin Solid Films,* 2014, vol. 570, p. 256. https://doi.org/10.1016/j.tsf.2014.05.019
17. Krysina, O.V., Ivanov, Yu.F., Prokopenko, N.A., Shugurov, V.V., et al., Influence of Nb addition on the structure, composition and properties of single-layered ZrN-based coatings obtained by vacuum-arc deposition method, *Surf. Coat. Technol.,* 2020, vol. 387, p. 125555. https://doi.org/10.1016/j.surfcoat.2020.125555
18. Qian, J., Zhou, F., Li, K., Wang, Q., et al., Optimization of deposition parameters and performance analysis of Nb-Zr-N composite films, *Surf. Coat. Technol.,* 2023, vol. 466, p. 129641. https://doi.org/10.1016/j.surfcoat.2023.129641

19. Krysina, O.V., Prokopenko, N.A., Ivanov, Yu.F., Tolkachev, O.S., et al., Multi-layered gradient (Zr,Nb)N coatings deposited by the vacuum-arc method, *Surf. Coat. Technol.,* 2020, vol. 393, p. 125759. https://doi.org/10.1016/j.surfcoat.2020.125759
20. Atar, E., Kayali, E.S., and Cimenoglu, H., Sliding wear behaviour of ZrN and (Zr, 12 wt % Hf)N coatings, *Tribol. Int.*, 2006, vol. 39, p. 297. https://doi.org/10.1016/j.triboint.2005.01.038
21. Atar, E., Kayali, E.S., and Cimenoglu, H., Reciprocating wear behaviour of (Zr, Hf)N coatings, *Wear,* 2004, vol. 257, p. 633. https://doi.org/10.1016/j.wear.2004.03.005
22. Atar, E., Cimenoglu, H.C., and Kayali, E.S., Hardness characterisation of thin Zr(Hf,N) coatings, *Surf. Coat. Technol.,* 2003, vol. 162, p. 167. https://doi.org/10.1016/S0257-8972(02)00558-3
23. Wu, Z.T., Qi, Z.B., Zhang, D.F., and Wang, Z.C., Microstructure, mechanical properties and oxidation resistance of (Zr, Hf)Nx coatings by magnetron co-sputtering, *Surf. Coat. Technol.,* 2015, vol. 276, p. 219. https://doi.org/10.1016/j.surfcoat.2015.06.071
24. Atar, E., Sarioglu, C., Cimenoglu, H., and Kayali, E.S., Residual stresses in (Zr,Hf)N films (up to 11.9 at % Hf) measured by X-ray diffraction using experimentally calculated XECs, *Surf. Coat. Technol.,* 2005, vol. 191, p. 188. https://doi.org/10.1016/j.surfcoat.2004.02.024
25. Cotrut, C.M., Braic, V., Balaceanu, M., Titorencu, I., et al., Corrosion resistance, mechanical properties and biocompatibility of Hf-containing ZrCN coatings, *Thin Solid Films,* 2013, vol. 538, p. 48. https://doi.org/10.1016/j.tsf.2012.12.100
26. Cherenda, N.N., Grigoriev, S.N., Basalai, A.V., Petukh, A.B., et al., Comparative study of mechanical and corrosion properties of coating on the basis of ZrN and TiN solid solutions, *High Temp. Mater. Proc.,* 2025, vol. 29, p. 35. https://doi.org/10.1615/HighTempMat-Proc.2024057613
27. Grigoriev, S., Vereschaka, A., Uglov, V., Milovich, F., et al., Influence of the tribological properties of the Zr,Hf-(Zr,Hf)N-(Zr,Me,Hf,Al)N coatings (where Me is Mo, Ti, or Cr) with a nanostructured wear-resistant layer on their wear pattern during turning of steel, *Wear,* 2023, vol. 518, p. 204624. https://doi.org/10.1016/j.wear.2023.204624
28. Vereschaka, A., Tabakov, V., Grigoriev, S., Sitnikov, N., et al., Investigation of the influence of the thickness of nanolayers in wear-resistant layers of Ti-TiN-(Ti,Cr,Al)N coating on destruction in the cutting and wear of carbide cutting tools, *Surf. Coat. Technol.,* 2020, vol. 385, p. 125402. https://doi.org/10.1016/j.surfcoat.2020.125402
29. Vereschaka, A., Cherenda, N., Sotova, C., Uglov, V., et al., Development of multicomponent nanostructured nitride coatings to protect against corrosion products from titanium alloy, *Coatings,* 2023, vol. 13, p. 2028. https://doi.org/10.3390/coatings13122028
30. Randall, N.X., The current state-of-the-art in scratch testing of coated systems, *Surf. Coat. Technol.,* 2019, vol. 380, p. 125092. https://doi.org/10.1016/j.surfcoat.2019.125092
31. Cherenda, N.N., Petukh, A.B., Kuleshov, A.K., Rusalsky, D.P., et al., Scratch testing of ZrN coating on Ti-6Al-4V titanium alloy surface preliminary treated by compression plasma flows impact, *High Temp. Mater. Process.,* 2024, vol. 28, p. 25. https://doi.org/10.1615/HighTempMat-Proc.2023051420
32. Cao, H., Ouyang, X., Wu, X., Chen, L., et al., Mechanical and electrochemical properties of titanium aluminum nitride coatings with different nitrogen flow rates on CrMnSi steel by filter cathode vacuum arc technology, *Coatings,* 2025, vol. 15, p. 379. https://doi.org/10.3390/coatings15040379